IEEE Access
Multidisciplinary | Rapid Review | Open Access Journal

Received March 5, 2019, accepted May 15, 2019, date of publication May 22, 2019, date of current version June 7, 2019.

Digital Object Identifier 10.1109/ACCESS.2019.2918263

Multiscale Contour Steered Region Integral and Its Application for Cultivar Classification

XIAOHAN YU[1,2], (Student Member, IEEE), YONGSHENG GAO[1], (Senior Member, IEEE), SHENGWU XIONG[2], AND XIAOHUI YUAN[2]

[1]School of Engineering, Griffith University, Brisbane, QLD 4111, Australia
[2]School of Computer Science and Technology, Wuhan University of Technology, Wuhan 430070, China

Corresponding author: Yongsheng Gao (yongsheng.gao@griffith.edu.au)

This work was supported in part by the Australian Research Council under Linkage Grant LP150100658, and in part by the National Key Research and Development Program of China under Grant 2016YFD0101900.

ABSTRACT In this paper, a multiscale contour steered region integral (MCSRI) method is proposed to classify highly similar shapes with flexible interior connection architectures. A component distance map (CDM) is developed to robustly characterize the flexible interior connection structure, shape of the exterior contour, and their inter-relationship in a shape image. A novel multiscale region transform (MReT) is proposed to perform region integral over different contour-steered strips at all possible scales to effectively integrate patch features, and thus enables a better description of the shape image in a coarse-to-fine manner. It is applied to solve a challenging problem of classifying cultivars from leaf images, which is a new attempt in both biology and computer vision research communities. A soybean cultivar leaf vein database (SoyCultivarVein), which is the first cultivar leaf vein database, is created and presented for performance evaluation. The experimental results demonstrate the superiority of the proposed method over the state-of-the-art methods in similar shape classification and the possibility of cultivar recognition via leaf pattern analysis, which may lead to a new research interest towards fine-level shape analysis on cultivar classification.

INDEX TERMS Cultivar classification, multiscale region transform, component distance map, structure pattern analysis.

I. INTRODUCTION

Soybean, one of the most essential global sources for protein and oil, is now the first legume species with a complete genome sequence [1]. Soybean cultivar classification is the first key step to facilitate soybean phenotype improvement needed for sustainable human and animal food production, energy production and environmental balance in agriculture worldwide. Given the vital role of soybean in ecosystem and agriculture, developing accurate and automatic cultivar classification approaches is of significant importance for both biology and computer vision research communities. This paper attempts to provide technical solutions to address the challenging cultivar classification problem, while acknowledging that our work is a first significant exploration for the specific soybean cultivar classification from leaf images.

The associate editor coordinating the review of this manuscript and approving it for publication was Yi Shang.

Many researchers have made great efforts on plant species classification by matching leaf images mainly represented by contour and vein features [2], [3]. The most common similarity classification approaches tested on general leaf image databases are based on the contour feature representations [4]–[9]. These contour-based methods yield desirable performances of plant species classification and retrieval on various publicly available leaf image databases. However, these methods fail to function when classifying cultivars, which is much more challenging than classifying species due to the fact that all cultivars belong to the same species. In other words, only utilizing the contour features may not provide sufficiently discriminative description of the leaf images for classifying cultivars in fine-level with similar shapes.

To address the insufficient description of solely using contour features, vein-based methods [10], [11] have been proposed for species identification from leaf images due to the vein structure diversity across species [12]. As stated in biology research community [13], [14], leaf architecture

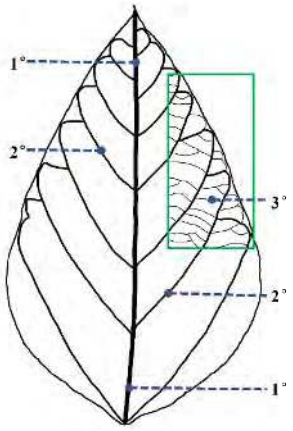

FIGURE 1. An example of soybean leaf veins, where 1° represents major vein, 2° denotes secondary vein, and 3° depicts tertiary vein.

describes definite structural patterns organized from elements of leaves, and can be coarsely classified into major vein, secondary vein and tertiary vein, as illustrated in Fig. 1. A major supportive reason for using vein features is that species differ strongly in leaf venation architecture [15]–[17]. Unfortunately, the above vein-based leaf recognition methods only demonstrate an applicability to species classification with obvious vein type variance, thus, cannot be applied to cultivar classification where all cultivars own the same vein type (e.g. the pinnate vein type for soybean cultivars) according to the vein type definition in their work. To overcome the limitations of above coarse-level vein type classification, Larese *et al.* [18] proposed a fine-level vein feature representation, for the first time, to address legume classification (soybean, red bean, and white bean). And then extended their method to the challenging cultivar classification to classify three soybean cultivars [19], a step closer to cultivar classification. Their inspiring work indeed demonstrates the importance of vein structure in legume level classification and the potential for further cultivar classification.

In this paper, we report our effort in confirming the possibility of cultivar recognition from leaf images, and a new method that may lead to advancement of pattern analysis research from species recognition to a new area of cultivar recognition. We proposed a multiscale contour steered region integral method to analyze the patch distance maps formed by the veins and the contour of a leaf. A new Multiscale Region Transform (MReT) is proposed, which can overcome the limitation of widely used line integral transforms (such as Radon Transform) in better encoding not only global features but also local features within a shape. A component distance map construction process is developed to robustly characterize the flexible interior connection structure, shape of the exterior contour, and their inter-relationship in a shape image. The very encouraging experimental results demonstrate the availability of cultivar information in leaf images and the effectiveness of the proposed method for cultivar identification, which may advance the research in leaf shape recognition from species to cultivar. In addition, a first soybean cultivar leaf vein database, which contains leaf images of 100 cultivars, is created and reported in this paper.

The rest of the paper is organized as follows. A brief review of related work is presented in Section II. Section III describes the details of the proposed multiscale contour steered region integral method. The experimental results and analysis on the first soybean cultivar vein database are presented in Section IV. Finally, the paper concludes in Section V.

II. RELATED WORK

Plant species classification from leaf images has received considerable attention from researchers in the past few decades [7], [8], [20]–[25]. Utilizing leaf images to classify the plant species is mainly due to the fact that leaf features are much more persistent and universal among the organs of plants [26]. The most recent leaf-related work proposed by Yin *et al.* [27] focuses on the multi-leaf segmentation, alignment and tracking problems. Considering the essential importance for high-throughput plant phenotyping study, an automatic image analysis method for Arabidopsis, which is the first plant with sequenced genome [28], is proposed. They closely connect the computer vision community and biology community for further comprehensive exploration in automatic plant classification and phenotype improvement. Similarly, we focus on the soybean because soybean is one of the most important crop plants, especially for its essential role in seed protein, oil content, and its capacity to fix atmospheric nitrogen. In addition, soybean genome has been sequenced with predicted protein-coding genes 70% more than the Arabidopsis [1], which may facilitate finding the connection between the genotype and phenotype of soybean to further improve the soybean cultivars.

Given the wealth of existing work on leaf contour-based shape classification, we naturally follow and investigate several popular algorithms that have been proven effective in leaf image classification. The most common contour-based approaches are based on pairwise similarity measures in which the matching costs are computed between a given pair of shapes. In these methods, feature representations extracted from each sampled contour point are designed to establish the robust correspondence [29]. Belongie *et al.* [4] developed a very effective shape descriptor, shape contexts (SC), which is widely used as a state-of-the-art benchmark. In their proposed descriptor, a histogram is attached to each boundary point for describing the relative distribution of the remaining points to that point. The matching is formulated as finding the correspondence in a point-by-point manner. Ling and Jacobs [5] proposed a powerful inner-distance shape contexts (IDSC) method, which is an improved form of the SC by using the length of the shortest path between two boundary points within the shape boundary. Dynamic Programming (DP) is also included for the shape matching after calculating the IDSC distance. Wang *et al.* [9] proposed a height functions (HF) method, in which the distance between the tangent line of each contour point and the other remaining contour points are calculated as the height function. Their descriptor

is designed to be robust and compact with invariances to translation, rotation and scaling. In the matching stage, they employed the DP algorithm for searching the optimal correspondence between sample points of two shapes. Srivastava *et al.* [6] introduced an important contour-based method which represents the shapes of curves using a square-root velocity (SRV) method. Through a gradient-based iteration process that is named as path straightening, the geodesics between shapes of closed elastic curves can be determined and thus be utilized for shape matching. In [30], they applied their method to the plant species classification and obtained excellent results on three publicly available plant species leaf databases (MAP score of 92.37% on Flavia [31], Nearest Neighbor score of 99.18% on Swedish [32] and identification score of 95.3% on ImageCLEF2011 [33]).

To further enhance the discriminative ability of contour representation from global information to local details, multiscale strategies are employed in recently proposed methods. Hu *et al.* [8] proposed a Multiscale Distance Matrix (MDM) method for plant species leaf recognition, in which the distances between sampled contour points are calculated in each scale to form the distance matrix. They also extended the MDM to be combined with other distances (e.g. inner-distance) to further explore their discriminability. Wang and Gao [7] presented a hierarchical string cuts (HSC) method to partition a contour into multiple scaled curve segments to describe a shape. The shape is described with global information and local details using geometric features from the partitioned shape segments. The abovementioned contour-based methods yield desirable results on plant species leaf classification. However, one of their fundamental limitations is that the interior information inside the shape is ignored. More precisely, the vein structure in a leaf is not considered.

Larese *et al.* [18] proposed an automatic procedure for legume classification (soybean, red bean and white bean) based only on the analysis of the leaf vein morphological features. Using LEAF GUI [34], they extract local features of the median, minimum and maximum values of 16 features such as vein length and vein orientation ($16 \times 3 = 48$ features), and 4 global features to form 52 features in total for leaf description. Encouraging results on three legume classification are reported, which demonstrate the importance of vein structure in leaf legume classification. In [19], they also applied the same method to classify three soybean cultivars, and obtained average classification accuracies ranging from 55.04% to 58.76%, which outperform the average classification accuracy of human experts (41.56% [19]). More studies associated with plant species identification can be found in [3].

III. MULTISCALE CONTOUR STEERED REGION INTEGRAL METHOD

In this section, a multiscale contour steered region integral (MCSRI) method is proposed for fine-level structure pattern analysis. To facilitate the MCSRI, a component distance map (CDM) is first developed, in which the interior structure, shape of the exterior contour, and their inter-relationship are characterized. A novel Multiscale Region Transform (MReT) is proposed to encode not only global features but also local structures within a shape. Then the algorithm for computing the discrete form MReT is presented. Finally, the similarity measure is defined using the transform coefficient matrices.

A. COMPONENT DISTANCE MAP

As a practical transform that attracts continuous research interest [35]–[39], the 2D Distance Transform (DT) can be defined as the calculation of a distance map in which the value of each pixel p is its minimum distance to a given set of pixels O in a binary image:

$$DT(p) = \min\{D(p, q), q \in O\}, \tag{1}$$

where D can be any L_p distance metric [39] (L_2 is used in this paper). By applying DT, the central part of a shape is assigned with higher value compared to the boundary or margin part which is more likely to be deformed. However, applying DT directly on the whole leaf shape encounters information loss of vein structure, as can be seen from Fig. 2(a).

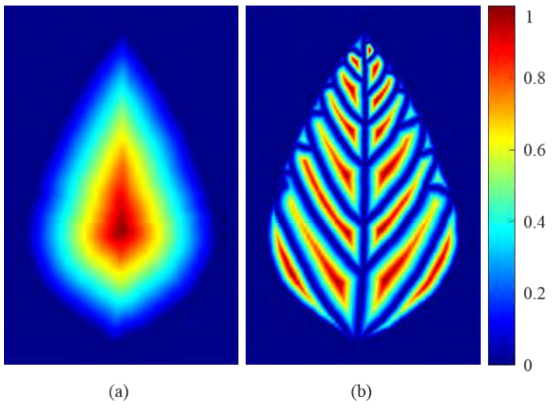

FIGURE 2. Visual comparison of distance map and component distance map of the leaf image shown in Fig. 1. (a) Distance map; (b) Component distance map.

To address the vein structure information loss problem, we propose to construct a component distance map (CDM) to characterize the vein structure, shape of the contour, and their inter-relationship in a leaf image. Veins and contour partition the leaf into two types of patches: vein patches and hybrid patches. Vein patches are the patches that are only enclosed by vein points, while hybrid patches are those enclosed by a mixture of vein points and leaf contour points. A leaf, $g(x, y)$, is composed of multiple various sized vein patches G_i^v and hybrid patches G_j^h, which can be represented as:

$$g(x, y) = \sum_{i=1}^{N^v} g_i^v(x, y) + \sum_{j=1}^{N^h} g_j^h(x, y), \tag{2}$$

where $g(x, y)$ is a labeled image, in which all pixels in a vein patch G_i^v and a hybrid patch G_j^h are labeled by a value of

i and a value of $N^v + j$, respectively. N^v and N^h are the numbers of vein patches and hybrid patches, respectively. $g_i^v(x, y)$ is defined to be i if $(x, y) \in G_i^v$, and 0 otherwise. Similarly, $g_j^h(x, y)$ is defined to be $N^v + j$ if $(x, y) \in G_j^h$, and 0 otherwise. The procedure of constructing the CDM of a leaf image is shown in Algorithm 1. Outputs $f_D^v(x, y)$ and $f_D^h(x, y)$ are vein and hybrid distance maps characterizing the vein structure and contour-vein relationship in a leaf image, respectively. Fig. 2(b) shows an example of the CDM of a soybean leaf image, in which the vein and hybrid distance maps are displayed together for easy observation.

Algorithm 1 Calculating Component Distance Map

Input:
$g(x, y)$: input labeled leaf image;
$g_i^v(x, y), i = 1, 2, \ldots, N^v$: vein patch functions;
$g_j^h(x, y), j = 1, 2, \ldots, N^h$: hybrid patch functions;
Function:
$\eta(m)$: compute the distance map by applying Eq. (1) on each non-zero point in matrix m;
Output:
$f_D^v(x, y)$: vein patch distance map;
$f_D^h(x, y)$: hybrid patch distance map;

1: **Initialize:**
Let $f_D^v(x, y)$ and $f_D^h(x, y)$ be zero matrices with the same size of input image $g(x, y)$;
2: **For** $i = 1$ **to** N^v
3: $f_D^v(x, y) = f_D^v(x, y) + \eta(g_i^v(x, y))$; (A1)
4: **End For**
5: **For** $j = 1$ **to** N^h
6: $f_D^h(x, y) = f_D^h(x, y) + \eta(g_j^h(x, y))$; (A2)
7: **End For**

B. MULTISCALE REGION TRANSFORM

Radon Transform (RT) [40] has been widely used [41]–[43] for capturing directional information of an image by calculating the line integral along a varying orientation. However, its integral over 1D line only represents global features but fails to provide local discriminative description of the shape, particularly those of interior structural patterns.

Here, we present a novel Multiscale Region Transform (MReT) to be applied on the CDM (refer to Section III.A), which can overcome the above limitation. By using the multiscale feature representation, the image region can be described in a coarse-to-fine manner to provide comprehensive description of the leaf image. More importantly, this allows encoding the inter-relationship of contour and interior context of a shape that can provide more discriminative power than the Radon transform. The proposed MReT transform and its use in shape description (see Fig. 3) are given as follows:

Definition 1: Given a contour point $p(u)$ (u ranges from 0 to 1), the arc length $l(t)$, from $p(u)$ to its end point $p(u, t)$ on the contour along clock-wise direction, is defined as $l(t) = P/2^t$, where P is the perimeter of contour, and t is the scale index ($t = 0, 1, \ldots, log_2 P$).

Definition 2: According to Definition 1, *the straight line passing through $p(u)$ and $p(u, t)$ is named as the base line and can be formulated as:*

$$L\left(\theta_u^t, \rho_u^t\right) = \left\{(x, y) \in \mathbb{R}^2 | x \sin\theta_u^t + y \cos\theta_u^t = \rho_u^t\right\}, \quad (3)$$

where ρ_u^t is the perpendicular distance from the origin to the base line $L\left(\theta_u^t, \rho_u^t\right)$. θ_u^t is the angle between the base line and the y-axis.

The yellow, purple, and red dashed lines in Figs. 3(f)-3(h) illustrate three examples of the base line at scales $t = 1, 2, 3$.

Definition 3: Given the base line $L\left(\theta_u^t, \rho_u^t\right)$ defined in Eq. (3), *a boundary line $L\left(\theta_u^t, \lambda_u^t\right)$, which is vertical to the base line is defined as*

$$L\left(\theta_u^t, \lambda_u^t\right) = \left\{(x, y) \in \mathbb{R}^2 | x \cos\theta_u^t + y \sin\theta_u^t = \lambda_u^t\right\}, \quad (4)$$

where λ_u^t is the perpendicular distance from the origin to the boundary line $L\left(\theta_u^t, \lambda_u^t\right)$.

When the boundary line $L\left(\theta_u^t, \lambda_u^t\right)$ scans along the base line from passing through $p(u)$ to the position of passing through $p(u, t)$, we can define a region integral transform as:

Definition 4: Let $p(u)$ and $p(u, t)$ be denoted by coordinates $(x(u), y(u))$ and $(x(u, t), y(u, t))$, a region integral on $p(u)$ at scale t is defined as:

$$\Phi_f^z\left(t, \theta_u^t\right) = \int_{-\infty}^{\infty} \int_{x(u)\cos\theta_u^t + y(u)\sin\theta_u^t}^{x(u,t)\cos\theta_u^t + y(u,t)\sin\theta_u^t} \int_{-\infty}^{\infty} \int_{-\infty}^{\infty} f_D^z(x, y)\, \delta\left(x \cos\theta_u^t + y \sin\theta_u^t - \lambda_u^t, x \sin\theta_u^t + y \cos\theta_u^t - \rho_u^t\right) dx dy d\lambda_u^t d\rho_u^t, \quad (5)$$

where $z = h, v$ and $\delta(\phi, \chi)$ is the 2D Dirac delta function defined as

$$\delta(\phi, \chi) = \begin{cases} 1, & \text{if } \phi = \chi = 0 \\ 0, & \text{otherwise} \end{cases} \quad (6)$$

The MReT on a given function $f_D^z(x, y)$ at point $p(u)$ is defined as

$$MReT\ (\theta_u)_f^z = \left[\Phi_f^z\left(0, \theta_u^0\right), \Phi_f^z\left(1, \theta_u^1\right), \ldots, \Phi_f^z\left(log_2 P, \theta_u^{log_2 P}\right)\right]^T. \quad (7)$$

The MReT transform at a single point $p(u)$ generates a vector of $(log_2 P + 1)$ coefficients with each describing the region integral for one scale at point $p(u)$. By moving $p(u)$ along the contour for a complete loop, which results in a varying $\theta \in [0, 2\pi)$, the above vector grows into a MReT coefficient

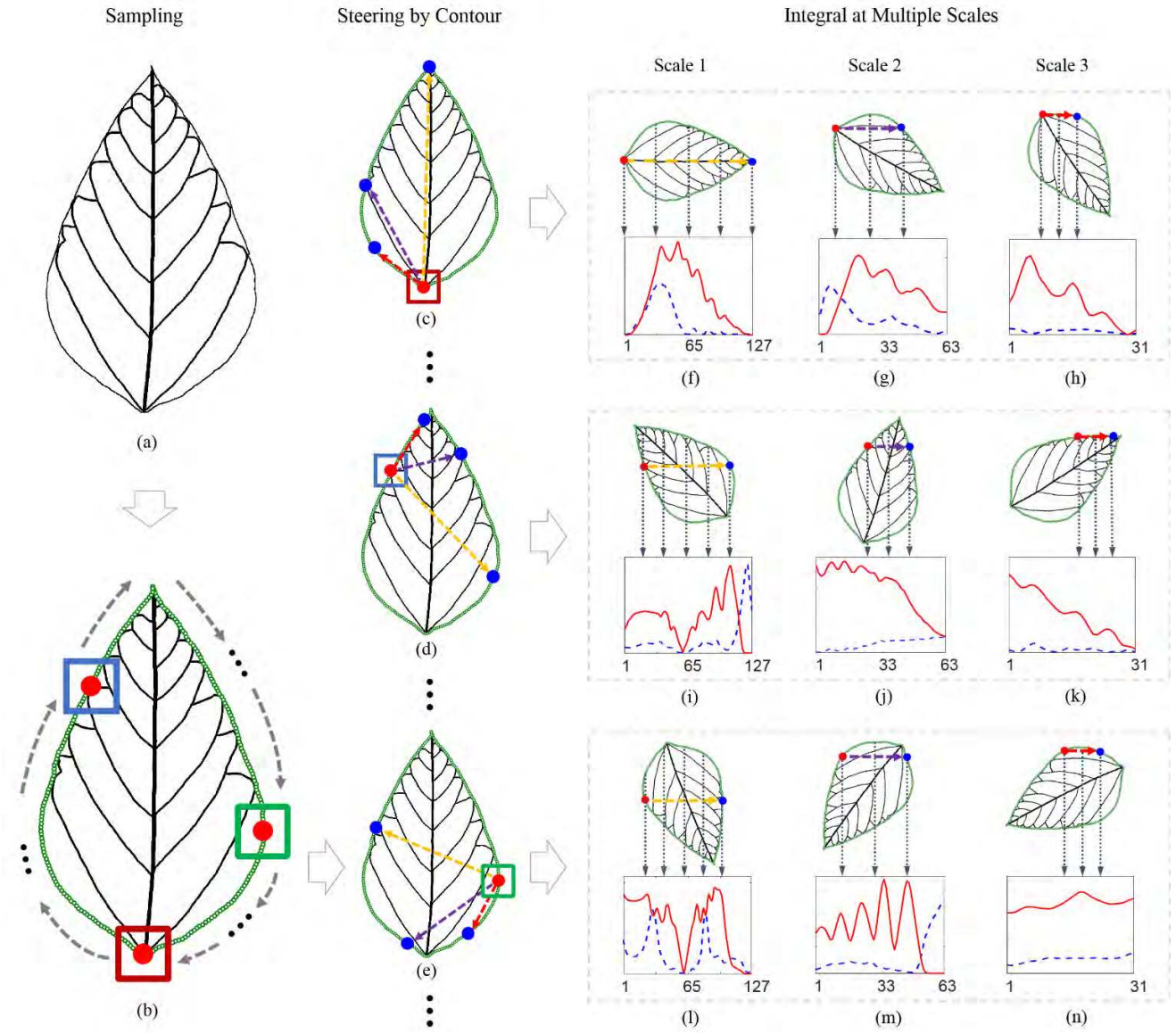

FIGURE 3. An example illustrating the process of the proposed multiscale region transform. (a) Input image. (b) Uniformly sampled contour (N = 256) with three example locations of a moving $p(u)$ point. (c), (d) and (e): Base lines (indicating the orientations of the region integral) for scales 1, 2 and 3 (shown in yellow, purple and red respectively) for the three example locations of $p(u)$ shown in (b). (f), (g) and (h) display the scanning ranges of the region integral for the $p(u)$ shown in (c) at scales 1, 2, and 3, respectively. (i), (j) and (k) display the scanning ranges of the region integral for the $p(u)$ shown in (d) at scales 1, 2, and 3, respectively. (l), (m) and (n) display the scanning ranges of the region integral for the $p(u)$ shown in (e) at scales 1, 2, and 3, respectively. From (f) to (n): The curves in red and blue display the line integral values along the boundary line on $f_D^v(x, y)$ and $f_D^h(x, y)$, respectively.

matrix of $(log_2 P+1)$ by P dimensions:

$$\boldsymbol{MReT}_f^z = \begin{bmatrix} \Phi_f^z\left(0, \theta_1^0\right) & \cdots & \Phi_f^z\left(0, \theta_P^0\right) \\ \Phi_f^z\left(1, \theta_1^1\right) & \cdots & \Phi_f^z\left(1, \theta_P^1\right) \\ \vdots & & \vdots \\ \Phi_f^z\left(log_2 P, \theta_1^{log_2 P}\right) & \cdots & \Phi_f^z\left(log_2 P, \theta_P^{log_2 P}\right) \end{bmatrix}. \tag{8}$$

This matrix describes how the region integrals at different scales synchronously vary when the point $p(u)$ moves.

As $p(u)$ moves along the contour, the region integral is performed over different regions defined by the scanning range and orientation of the boundary line at all possible scales. An example of the MReT process, that illustrates various orientations and ranges of the region integral on a moving $p(u)$ at different scales, is given in Fig. 3. When scale $t = 1, 2, \ldots$, $p(u)$ and $p(u, t)$ cut a half, a quarter, $\ldots$, off the contour to steer the region integral at different orientations. The greater the t is, the smaller integral region is scanned, which provides finer descriptions on local details of the target. When scale $t = 0$, $p(u)$ and $p(u, t)$ become the same point after a complete loop and thus the region

Algorithm 2 Selecting Points in Moving Integral Strips $R_f\left(t,\theta_i^t\right)$

Input:
$(x\,(i)\,,y\,(i))=p(i)$: start point of base line;
$(x\,(j)\,,y\,(j))=p(i,t)$: end point of base line;
(x,y): any point in CDM $f_D^z\,(x,y)$;
Output:

$$\text{Boolean}IN\,(x,y)=\begin{cases}1, & if\ (x,y)\in R_f\left(t,\theta_i^t\right)\\ 0, & otherwise;\end{cases}$$

1: Substitute x into Eqs. (9) and (10), respectively, and calculate

$$y_i=x\,(i)\cot\theta_i^t+y\,(i)-x\cot\theta_i^t \tag{A3}$$

and

$$y_j=x\,(j)\cot\theta_i^t+y\,(j)-x\cot\theta_i^t. \tag{A4}$$

2: **If** $(y_i-y)\cdot(y_j-y)\le 0$
3: $IN\,(x,y)=1$;
4: **else**
5: $IN\,(x,y)=0$;
6: **End If**

integral is performed over the whole region of the given image, making the first row elements in matrix $\boldsymbol{MReT}_f^z$ share the same value. The 2nd, 3rd, 4th rows in matrix $\boldsymbol{MReT}_f^z$ are visualized in the 3rd, 4th, and 5th columns of Fig. 3.

C. DISCRETE MReT

In this section, we present the algorithm of computing discrete Multiscale Region Transform.

First, the contour of the leaf is uniformly sampled into $N=2^8=256$ points, as illustrated by the process from Fig. 3(a) to Fig. 3(b). Then, for each sampled contour point $p(i)$, we compute the end points $p(i,t)$ for scales $t=0,1,\ldots,log_2N$. Based on the Definition 1 in Section III.B, the end points in discrete form become $p\,(i,N)\,,p\,(i,N/2)\,,\ldots,p\left(i,N/2^t\right),\ldots,p\,(i,1)$. Their arc lengths $l(t)$ become digitized as 256, 128, …, 1, for $N=256$ sampling.

In a numerical form, the start and end base line points on the contour (that is $p(u)$ and $p(u,t)$ defined in continuous forms in Definition 4) are digitized into $p\,(i)=(x(i),y(i))$ and $p\,(j)=(x(j),y(j))$. Then the points (x,y) on the two boundary lines passing through $p(i)$ and $p(j)$ can be determined by

$$x\cos\theta_i^t+y\sin\theta_i^t=x\,(i)\cos\theta_i^t+y\,(i)\sin\theta_i^t, \tag{9}$$

and

$$x\cos\theta_i^t+y\sin\theta_i^t=x\,(j)\cos\theta_i^t+y\,(j)\sin\theta_i^t, \tag{10}$$

respectively. The integral region of the proposed MReT transform, denoted as $R_f\left(t,\theta_i^t\right)$, is a strip between the above two boundary lines. The width, location, and orientation of the integral strip vary according to the scale t, location of the moving $p\,(i)$ along the contour, and baseline angle θ_i^t (see Figs. 3(f)-3(n)). We developed a fast algorithm (see

Algorithm 3 Computing Discrete Multiscale Region Transform

Input:
$f_D^v\,(x,y)$: vein patch distance map;
$f_D^h\,(x,y)$: hybrid patch distance map;
N: number of sampling points on contour;
Output:
$\boldsymbol{MReT}_f^v$: vein MReT coefficient matrix;
$\boldsymbol{MReT}_f^h$: hybrid MReT coefficient matrix;

1: Initialize the two MReT coefficient matrices as zero matrices:
$\boldsymbol{MReT}_f^v=\mathbf{0}_{(log_2N+1)\times N}$, $\boldsymbol{MReT}_f^h=\mathbf{0}_{(log_2N+1)\times N}$;
2: **For** $i=1$ **to** N
3: **For** $t=0$ **to** log_2N
4: Compute $(x\,(i)\,,y\,(i))=p(i)$ and $(x\,(j)\,,y\,(j))=p(i,t)$ using Definition 1;
5: **For** $k=1$ **to** N_f
6: Determine if the point (x_k,y_k) in a labeled image is inside the integral strip $R_f\left(t,\theta_i^t\right)$ using Algorithm 2;
7: **If** $IN\,(x_k,y_k)=1$
8:

$$\Phi_f^v\left(t,\theta_i^t\right)=\Phi_f^v\left(t,\theta_i^t\right)+f_D^v\,(x_k,y_k); \tag{A5}$$

9:

$$\Phi_f^h\left(t,\theta_i^t\right)=\Phi_f^h\left(t,\theta_i^t\right)+f_D^h\,(x_k,y_k); \tag{A6}$$

10: **End If**
11: **End For**
12: **End For**
13:

$$\boldsymbol{r}_i^v=[\Phi_f^v\left(0,\theta_i^0\right),..,\Phi_f^v\left(log_2N,\theta_i^{log_2N}\right)]^T; \tag{A7}$$

14:

$$\boldsymbol{r}_i^h=[\Phi_f^h\left(0,\theta_i^0\right),..,\Phi_f^h\left(log_2N,\theta_i^{log_2N}\right)]^T; \tag{A8}$$

15: **End For**
16:

$$\boldsymbol{MReT}_f^v=[\boldsymbol{r}_1^v,..,\boldsymbol{r}_N^v]; \tag{A9}$$

17:

$$\boldsymbol{MReT}_f^h=[\boldsymbol{r}_1^h,..,\boldsymbol{r}_N^h]; \tag{A10}$$

Algorithm 2) to efficiently determine whether a point in the image is located inside the moving integral strip $R_f\left(t,\theta_i^t\right)$, which will be used in Algorithm 3 for discrete MReT computation.

Let $\left\{(x_k,y_k)\,,k=1,\cdots,N_f\right\}$ be a subset of pixels in the image whose $g(x_k,y_k)\neq 0$ (refer to Eq. (2)). N_f is the total number of pixels enclosed in the leaf contour. The procedure of computing the discrete MReT coefficient matrix $\boldsymbol{MReT}_f^z$ is presented in Algorithm 3, in which Eq. (5) is transformed into the sum of label values in a moving integral strip $R_f\left(t,\theta_i^t\right)$. It is worth noting that when scale $t=0$, $p(i)$ and $p(j)$ become the same point and θ_i^t becomes an arbitrary angle, resulting in infinite number of boundary lines spanning all possible orientations. Thus, every region point (x_k,y_k) can be considered as being located on the boundary lines, which leads to $(y_i-y_k)\cdot(y_j-y_k)\equiv 0$ in Step 2 of Algorithm 2.

For a contour point $p(i)$, the discrete MReT generates two (log_2N+1) dimensional vectors:

$$\boldsymbol{r}_i^v = [\Phi_f^v\left(0,\theta_i^0\right),\ldots,\Phi_f^v\left(t,\theta_i^0\right),\ldots,\Phi_f^v\left(log_2N,\theta_i^{log_2N}\right)]^T, \tag{11}$$

and

$$\boldsymbol{r}_i^h = [\Phi_f^h\left(0,\theta_i^0\right),\ldots,\Phi_f^h\left(t,\theta_i^0\right),\ldots,\Phi_f^h\left(log_2N,\theta_i^{log_2N}\right)]^T. \tag{12}$$

By moving $p(i)$ along the contour for a complete loop, the two vectors grow into a pair of (log_2N+1)-by-N matrices $\boldsymbol{MReT}_f^v$ and $\boldsymbol{MReT}_f^h$ (see A9 and A10 in Algorithm 3). Because the size of the integral region for calculating an entry in $\boldsymbol{r}_i^z$ decreases when t increases (see Figs. 3(f)-(h)), $\Phi_f^z\left(t,\theta_i^0\right)$ is locally normalized by dividing its maximum value $\Phi_f^z\left(t,\theta_i^0\right)$ among all i. Because $\Phi_f^z\left(0,\theta_i^0\right)$ is a constant for all i, it is normalized by its mean obtained from a set of example leaf images.

As Steps 2, 3 and 5 take time $O(N)$, $O(log_2N)$ and $O(N_f)$ respectively, the algorithm 3 has a computational complexity of $O(N_f N log_2 N)$.

D. SIMILARITY MEASURE

Given two sets of matrices $\mathbf{T} = \bigcup_k \boldsymbol{MReT}_{f(T)\_k}^z = \left\{\boldsymbol{MReT}_{f(T)\_1}^z,\ldots,\boldsymbol{MReT}_{f(T)\_K}^z\right\}$ and $\mathbf{M} = \bigcup_k \boldsymbol{MReT}_{f(M)\_k}^z = \left\{\boldsymbol{MReT}_{f(M)\_1}^z,\ldots,\boldsymbol{MReT}_{f(M)\_K}^z\right\}$ representing the MReT coefficient matrices of the test and model cultivars respectively. Each matrix set is comprised of K matrix pairs of $\boldsymbol{MReT}_f^v$ and $\boldsymbol{MReT}_f^h$. K is the number of leaf types (In our experiments, K is set as 3 where $k=1$ denotes a upper part leaf, $k=2$ denotes a middle part leaf, and $k=3$ denotes a lower part leaf. Note that $\boldsymbol{MReT}_{f(T)\_k}^z$ in $\boldsymbol{T}$ can only be matched against the matrix of the same type in $\boldsymbol{M}$, that is $\boldsymbol{MReT}_{f(M)\_k}^z$ with the same leaf type index k.

$\boldsymbol{MReT}_f^z$ is rotation variant. When the initial location of the contour point, that steers the Multiscale Region Transform (i.e., the red boxed point in Fig. 3), moves clockwise, the entire column of $\boldsymbol{r}_i^z$ in $\boldsymbol{MReT}_f^z$ shifts to the right. The magnitudes of its 1D Fourier transform coefficients and 2D Fourier transform coefficients are calculated by

$$\tilde{\Phi}_1^z(t,k) = \left(\frac{1}{N}\right)\left|\sum_{i=1}^{N}\Phi_f^z\left(t,\theta_i^t\right)\exp\left(-\frac{j2\pi ik}{N}\right)\right|, \tag{13}$$

where $k=1,\ldots,N$ and $t=0,\ldots,log_2N$, and

$$\tilde{\Phi}_2^z(t,k) = \left(\frac{1}{Nlog_2N}\right)\left|\sum_{i=1}^{N}\sum_{\gamma=1}^{log_2N}\Phi_f^z\left(t,\theta_i^t\right)\times\exp\left(-j2\pi\left(\frac{ik}{N}+\frac{\gamma t}{log_2N}\right)\right)\right|, \tag{14}$$

where $k=1,\ldots,N$ and $t=1,\ldots,log_2N$. From theory, the above obtained $\tilde{\Phi}_1^z(t,k)$ and $\tilde{\Phi}_2^z(t,k)$ are invariant to the initial location of the contour point that steers the MReT, and thus invariant to rotation of the whole leaf. To make the generated feature descriptor robust to noise and compact, the lowest M order coefficients are used to describe the object (i.e., the soybean cultivar in this study), where $M \ll N$.

Both $\tilde{\Phi}_1^z(t,k)$ and $\tilde{\Phi}_2^z(t,k)$ are used to construct a feature descriptor as

$$\boldsymbol{\Psi}_f^z = \begin{bmatrix} \tilde{\Phi}_1^z(0,1) & \ldots & \tilde{\Phi}_1^z(0,M) \\ \tilde{\Phi}_1^z(1,1) & \ldots & \tilde{\Phi}_1^z(1,M) \\ \vdots & \ldots & \vdots \\ \tilde{\Phi}_1^z\left(log_2N,1\right) & & \tilde{\Phi}_1^z\left(log_2N,M\right) \\ \tilde{\Phi}_2^z(1,1) & \ldots & \tilde{\Phi}_2^z(1,M) \\ \vdots & \ldots & \vdots \\ \tilde{\Phi}_2^z\left(log_2N,1\right) & & \tilde{\Phi}_2^z\left(log_2N,M\right) \end{bmatrix}, \tag{15}$$

in which $\tilde{\Phi}_1^z(t,k)$, $k=0,\ldots,M$ are features invariant to rotation of the shape while $\tilde{\Phi}_2^z(t,k)$, $k=1,\ldots,M$ act as constrains that ensure $\boldsymbol{r}_i^v$ and $\boldsymbol{r}_i^h$ remain meaningful MReT vectors for each contour point $p(i)$. Thus, the test and model cultivars are represented by feature matrices $\boldsymbol{\Psi}_{f(T)}^z = \bigcup_k \boldsymbol{\Psi}_{f(T)\_k}^z = \left\{\boldsymbol{\Psi}_{f(T)\_1}^z,\ldots,\boldsymbol{\Psi}_{f(T)\_K}^z\right\}$ and $\boldsymbol{\Psi}_{f(M)}^z = \bigcup_k \boldsymbol{\Psi}_{f(M)\_k}^z = \left\{\boldsymbol{\Psi}_{f(M)\_1}^z,\ldots,\boldsymbol{\Psi}_{f(M)\_K}^z\right\}$, where $z=v,h$. Fig. 4 gives an example of illustrating the cultivar feature matrix construction process, and $\boldsymbol{\Psi}_f^z$ is visually displayed in Fig. 4(d).

The dissimilarity between two given cultivars can be measured using the fast L_1 Minkowski distance of the two matrices:

$$dis\left(\boldsymbol{\Psi}_{f(T)}^z,\boldsymbol{\Psi}_{f(M)}^z\right) = \sum_{k=1}^{K}\left[w\left|\boldsymbol{\Psi}_{f(T)_k}^v-\boldsymbol{\Psi}_{f(M)_k}^v\right|+\left|\boldsymbol{\Psi}_{f(T)_k}^h-\boldsymbol{\Psi}_{f(M)_k}^h\right|\right] \tag{16}$$

where w is a weight that balances the contributions of vein patches and hybrid patches in measuring the dissimilarity of soybean cultivar leaves.

IV. EXPERIMENTS AND DISCUSSIONS

To examine if the soybean leaf veins and shapes contain discriminative pattern information for identifying cultivars, experiments are conducted to evaluate the performance of the proposed method and compared with nine state-of-the-art leaf identification benchmark methods. They are: (1) vein trait method [18], [19], (2) two versions of Shape Contexts, i.e., standard Shape Contexts (SC) and Shape Contexts with dynamic programming (SC-DP) [4], (3) Inner Distance Shape Contexts (IDSC) and Inner Distance Shape Contexts with dynamic programming (IDSC-DP) [5], (4) square-root velocity (SRV) method [6], (5) Hierarchical String Cuts (HSC) [7], (6) Multiscale Distance Matrix (MDM) [8], and (7) Height Functions (HF) [9]. The widely used Nearest

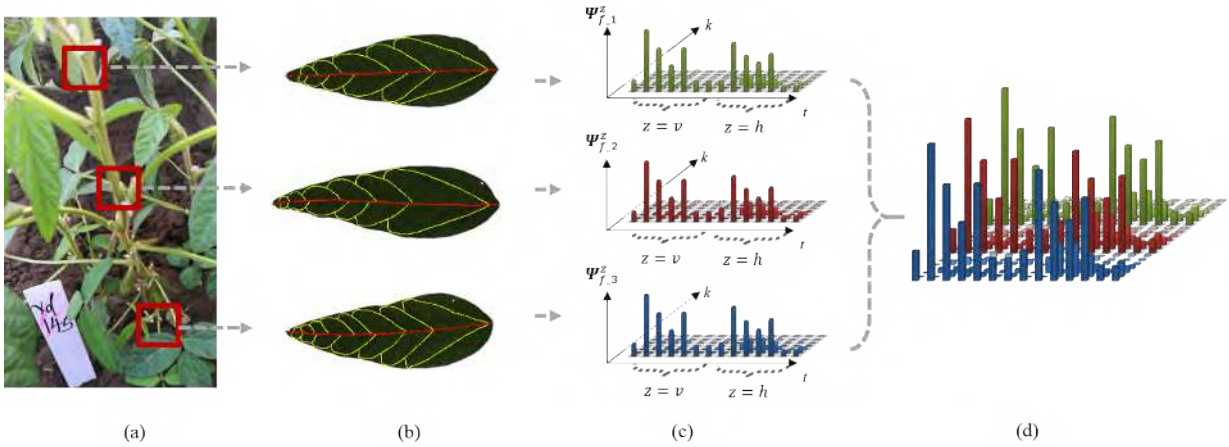

FIGURE 4. An example of illustrating the cultivar feature matrix construction process. (a) A soybean cultivar plant in the field. (b) Three example leaves collected from the upper, middle, and lower parts of the cultivar plant. (c) Feature matrices $\Psi^z_{f\_1}$, $\Psi^z_{f\_2}$, and $\Psi^z_{f\_3}$ calculated from the three leaf images in (b). (d) Feature matrix Ψ^z_f of the cultivar.

Neighbor score (1NN) [4]–[9], Cumulative Match Characteristic (CMC) curve [5], and bulls-eye test score [4], [5], [7], [9] are employed for performance measurement, as used in the benchmark methods. Score level fusion is used when implementing the benchmark algorithms for joint matching of the leaves from the upper, middle and lower parts. The code of the proposed MReT method is available online at https://maxwell.ict.griffith.edu.au/cvipl/demos/MRet2019.zip.

A. SOYBEAN CULTIVAR LEAF VEIN DATABASE

There is a growing sentiment in the pattern analysis and computer vision community to create image databases to cater for the need of advancing the research from species identification to more challenging fine-level cultivar identification. In this research, we built the first soybean cultivar leaf vein database, SoyCultivarVein, by collecting the leaf images from soybean plants of different cultivars. The SoyCultivarVein database[1] contains 600 leaves collected from plants of 100 soybean cultivars that grow in Jilin Province of China. For each cultivar, we randomly collected two cultivar samples with each sample containing a leaf from the upper part, a leaf from the middle part, and a leaf from the lower part of the plants. The transparent scans of the back side of the leaves are obtained using an EPSON V800 scanner with a resolution of 600 DPI and 24 bit true color setting.

Ground truth venation of the leaves are manually labeled using the botanic vein order classification method [13], [14]. It is worth noting that it is very difficult for human to distinguish cultivars due to the small inter-cultivar differences in comparison with their intra-cultivar variations (see examples in Fig. 5). Examples of leaf veins and contours from the 100 cultivars in the SoyCultivarVein database are shown in Fig. 6, in which each cultivar is represented by one of the upper part leaves. For some soybean cultivars, their leaves from different parts of the plants exhibit a quite diverse appearance in completely different shapes, while for other soybean cultivars, their leaves from different parts of the plants have the same shape. However, compared to the species leaf image databases Leaf100 [7], MEW2012 [45], ICL [8], the leaves in the SoyCultivarVein database are highly similar due to the fact that they all belong to the same species, making it a new and challenging dataset for the artificial intelligence and pattern analysis research community.

[1]Database available at https://maxwell.ict.griffith.edu.au/cvipl/databases/SoyCultivarVein_Dataset.7z

B. DETERMINATION OF PARAMETER

In this section, we investigate the effect and sensitivity of parameter w in Eq. (16) on the recognition accuracy. In theory, the parameter w is a weight used to balance the contributions from the vein patches and the hybrid patches. Fifty cultivars randomly selected from the SoyCultivarVein database were used in our parameter sensitivity analysis. We randomly select one sample from each cultivar to construct a testing dataset, and the remaining samples are used as the model dataset. The experiment of nearest neighbor classification (1NN) [4]–[9] is repeated 1000 times. The average recognition accuracies of the proposed method are plotted against the values of w in Fig. 7.

It is observed that, the average accuracy of the proposed method is 50.13% when $w = 0$ (that is only using hybrid patches). It increases quickly with the increase of w and then remains higher than 60% with w ranging from 0.7 till $+\infty$. It is also worth noting that, when the parameter w becomes infinite (that is only using vein patches), the average classification accuracy still remains 62.51%, confirming the significance of the vein structure information in cultivar classification. For the rest of the experiments in this paper, we set w as 4.5 for both the proposed method and the proposed method using additional 3° veins.

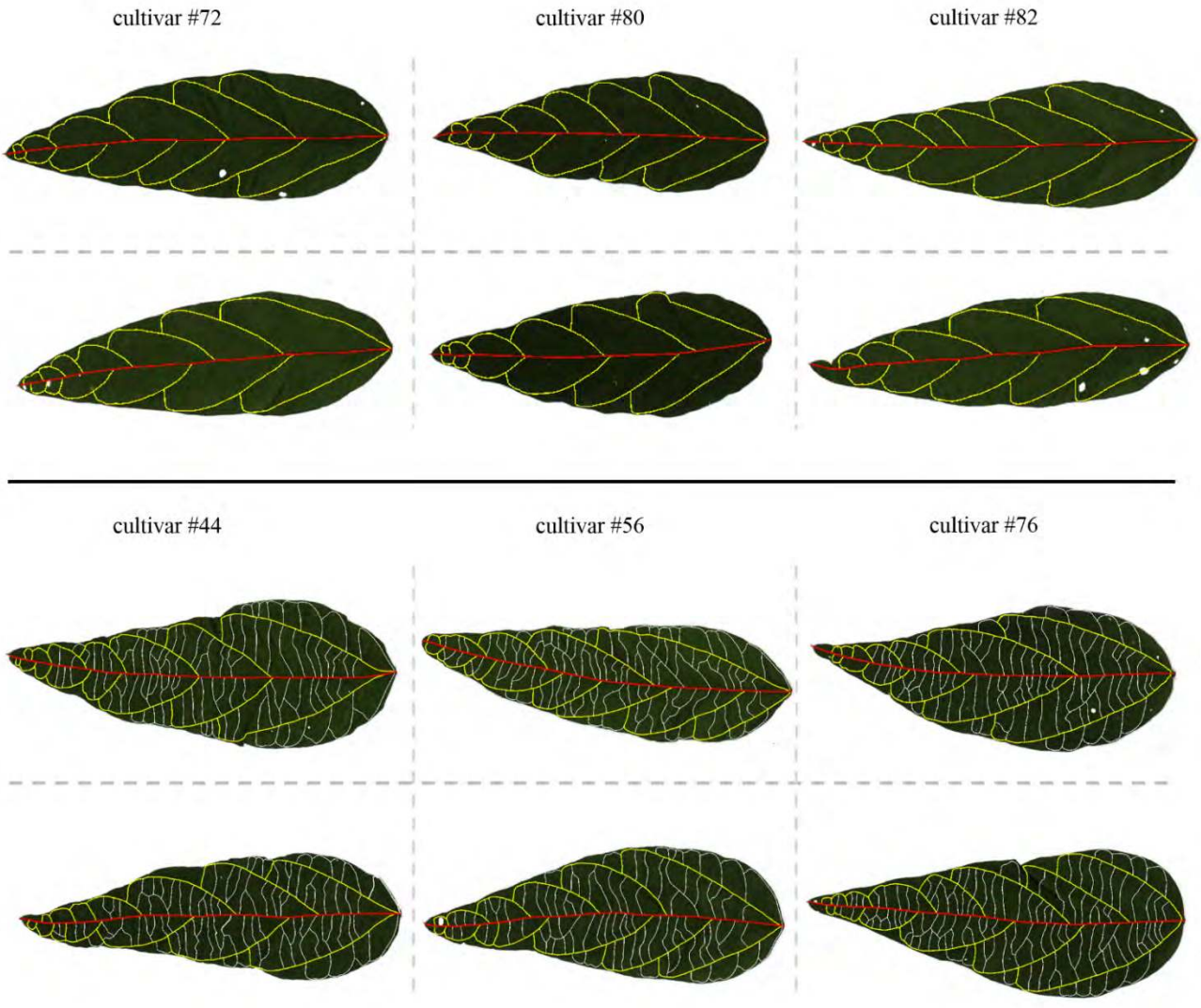

FIGURE 5. Examples illustrating the small inter-cultivar differences (compare contours and veins horizontally) in comparison to their intra-cultivar variations (compare contours and veins vertically) in SoyCultivarVein database. The second row also displays the tertiary veins provided in the database.

C. COMPARISON WITH FINE-LEVEL LEAF CLASSIFICATION METHOD

In this section, we compare the performance of the proposed method against the only fine-level leaf classification method [18], [19], which explored leaf classification among three legumes and three cultivars. For a fair comparison, we first use the same small-class classification protocol as in [19] by randomly selecting three cultivars from the SoyCultivarVein database for our experimental tests. We repeat the experimental test 100 times by each time randomly re-electing three cultivars from the SoyCultivarVein database. For each three-cultivar classification test, the same 1NN protocol as in Section IV.B is used for computing the average classification accuracy. The average classification accuracies of the competing methods are tabulated in Table 1. The proposed method achieved an average classification accuracy of 96.24%, which is significantly higher than the 57.30% accuracy of the benchmark [19]. It is noted that, the performance of the vein trait method [19] (57.30%) obtained from our randomly selected three-cultivar test is close to the classification accuracy range (55.04% to 58.76%) reported in [19], confirming the reliability of the result in [19] on a different database. We also examine the discriminative ability of the tertiary veins for cultivar classification. In the second experiment, the tertiary veins are used to further partition the patches. The proposed method using additional 3° veins achieved an average classification accuracy of 96.61%, slightly higher (0.37%) than the proposed method using major and secondary veins.

Another series of experiments are conducted by increasing the number of soybean cultivars from 10 to 100 with a step size of 10. The experimental test is repeated 100 times by

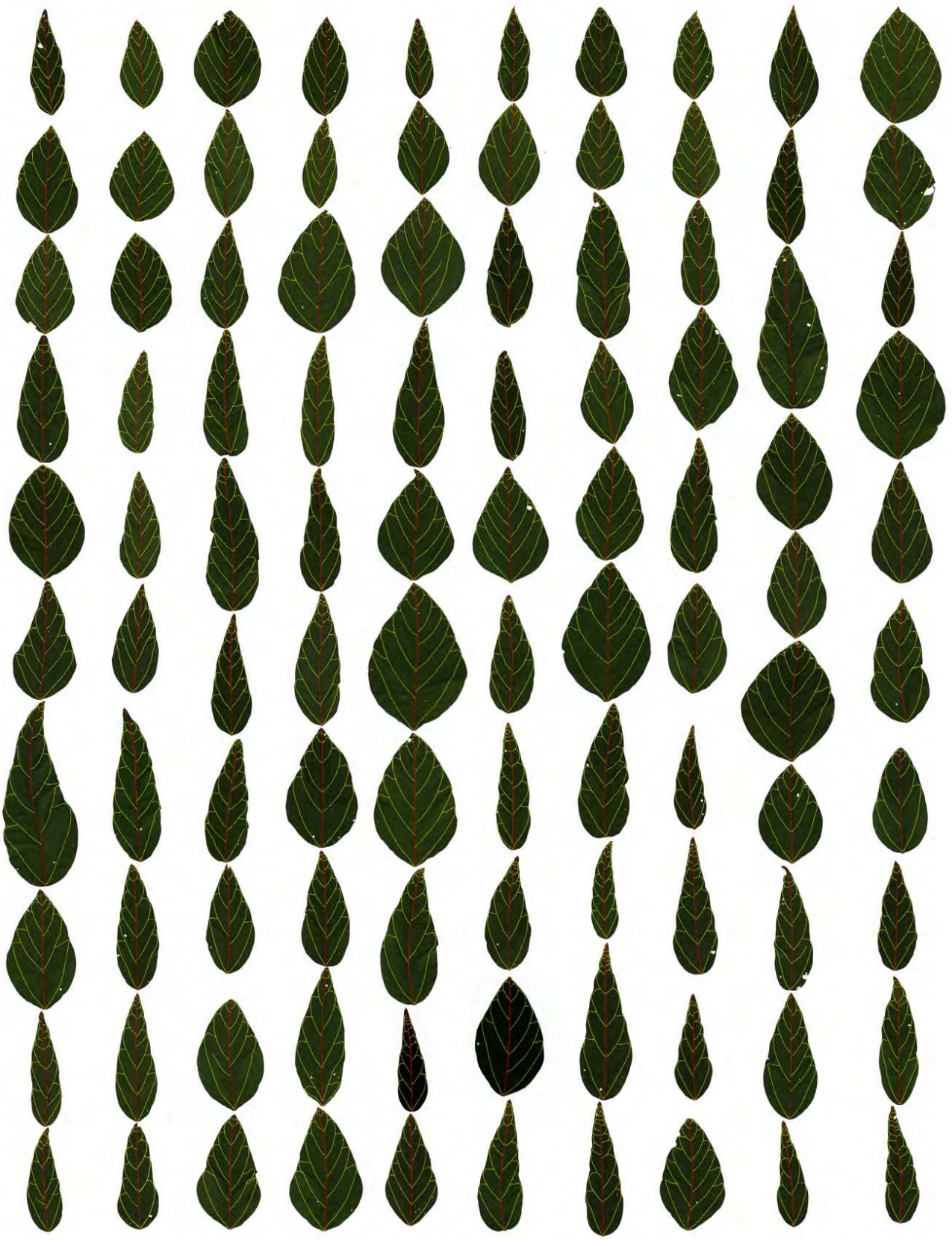

FIGURE 6. Examples of leaf vein images from the 100 cultivars in the SoyCultivarVein database. One upper part leaf per cultivar is shown as an example.

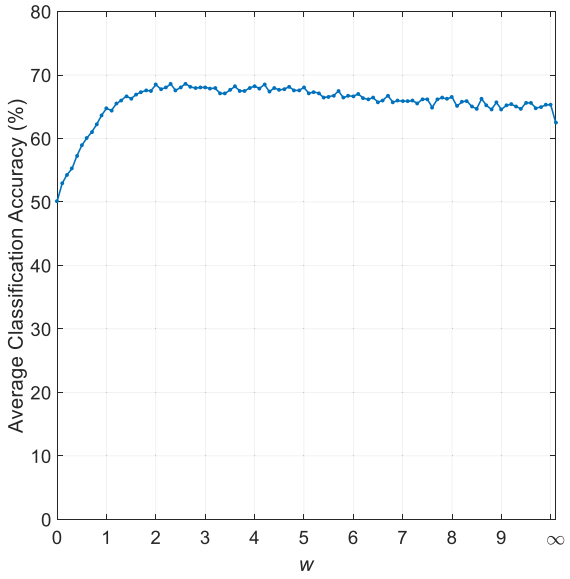

FIGURE 7. Average classification accuracy versus parameter w.

TABLE 1. Average classification accuracy on three-cultivar subset of SoyCultivarVein database ($M = 7, t_{max} = 3$).

Algorithm	Nearest Neighbor Score (%)
Vein trait method [18], [19]	57.30
Proposed method	**96.24**
Proposed method (+3° vein)	**96.61**

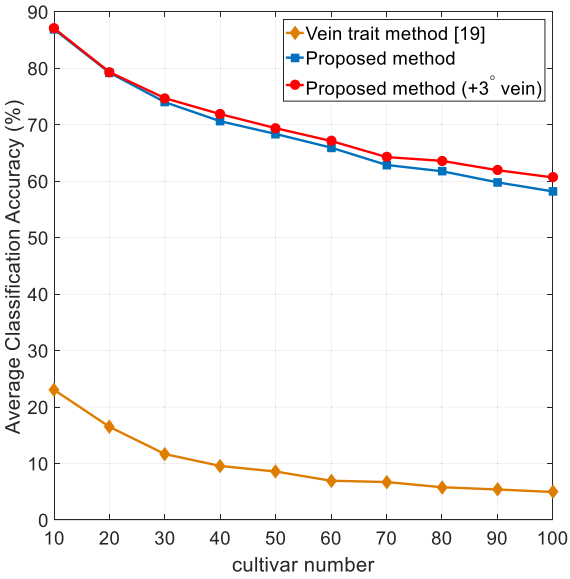

FIGURE 8. Average classification accuracies using varying number of cultivars from SoyCultivarVein database.

reselecting different cultivars randomly from the SoyCultivarVein database. The average classification accuracies of the proposed method and the benchmark method are plotted against an increasing number of cultivars in Fig. 8. It is encouraging to observe that the proposed method consistently outperform the benchmark method with a large margin. When the number of the soybean cultivars increases from 10 to 100, the average classification accuracy of the proposed method drops from 86.87% to 58.19% (the proposed method using additional 3° veins drops from 87.05% to 60.67%), while the accuracies of the benchmark approach decreases from 23.03% to 4.96%.

D. COMPARISON WITH SPECIES CLASSIFICATION METHODS

In this section, we compare the proposed method with the state-of-the-art contour-based benchmarks (SC [4], IDSC [5], SRV [6], HSC [7], MDM [8], and HF [9]) on all the 600 leaves of 100 cultivars in the SoyCultivarVein database.

TABLE 2. Average classification accuracy on SoyCultivarVein database ($M = 7, t_{max} = 3$).

Algorithm	Nearest Neighbor Score (%)
SC [4]	37.58
SC+DP [4]	36.90
IDSC [5]	49.07
IDSC+DP [5]	46.93
SRV [6]	37.09
HSC [7]	43.98
MDM [8]	39.39
HF [9]	40.46
Proposed method	**58.19**
Proposed method (+3° vein)	**60.67**

1) CLASSIFICATION TEST

Table 2 illustrates the average classification results of the proposed approach together with the state-of-the-art contour-based methods. Using the same evaluation setting as used in Section 4.2, the proposed method achieves the highest classification accuracies of 58.19% and 60.67% (using additional 3° veins) respectively, which are significantly higher than the state-of-the-art benchmarks. Given the success of above benchmarks in species leaf classification, these results demonstrate the effectiveness and superiority of the proposed method in cultivar classification.

2) CUMULATIVE PERFORMANCE TEST

To further compare the cumulative performance of classification rather than presenting a single classification rate for each competing method, we employ the Cumulative Match Characteristic (CMC) curve [44]–[47] to evaluate the performance of proposed method against the benchmarks. For each soybean cultivar, there are two samples in the SoyCultivarVein database. We randomly select one sample from each cultivar to construct a test dataset, and the remaining samples are used as the model dataset. Each sample in the test dataset is matched against all the samples in the model dataset, which results in 100 matching tests. The classification evaluation is repeated 1000 times by reselecting different samples randomly from the SoyCultivarVein database to construct the test and model datasets. The CMC curve, at rank N,

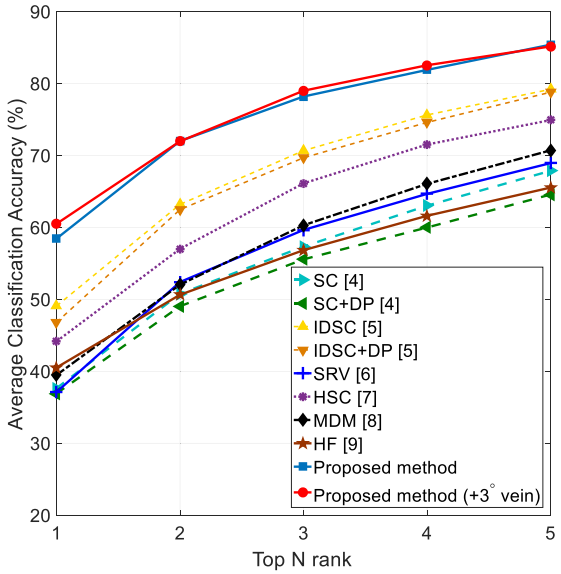

FIGURE 9. CMC curves of all the competing methods on the whole SoyCultivarVein database.

calculates the average percentage (of the 1000 repeats) of the test samples whose correct match (that is the test sample and the model sample belong to the same cultivar) is among the top N best matches [48]. The CMC curves of the proposed method and the state-of-the-art approaches, including SC [4], SC + DP [4], IDSC [5], IDSC + DP [5], SRV [6], HSC [7], MDM [8], and HF [9], are shown in Fig. 9. It can be seen that the CMC curve of the proposed method is higher than all the benchmark methods with a large margin of over 10% in accuracy. The consistent superiority of the proposed method against the state-of-the-art methods reconfirms the discriminative ability of the proposed method in fine-level cultivar pattern classification. The very small margin between the proposed method and the proposed method using additional 3° veins as shown in CMC curves indicates that the tertiary veins may not provide more additional discriminative information over the secondary veins for cultivar classification.

3) IMAGE RETRIEVAL TEST

Comparative experiments are also conducted using the bulls-eye test score measurement for image retrieval tasks [4], [5], [7], [9], [48]–[52]. In this retrieval test, each query sample is matched against all the samples in the SoyCultivarVein database. The number of correct matches (that is the retrieved sample and the query sample belong to the same cultivar) in the top 2 × T (where T is the number of samples in the database that belong to the same cultivar of the query sample) retrieved samples that have the smallest dissimilarity values are counted. The average percentage of matched samples out of T over all the queries is the bulls-eye test score [5]. Since there are two samples for each cultivar in the SoyCultivarVein database, T = 2 in this experiment. As can be seen from Table 3, the proposed method achieves

TABLE 3. Image retrieval rate on SoyCultivarVein database ($M = 7, t_{max} = 3$).

Algorithm	Bulls-eye Test Score (%)
SC [4]	73.75
SC+DP [4]	74.25
IDSC [5]	80.00
IDSC+DP [5]	80.75
SRV [6]	74.75
HSC [7]	77.50
MDM [8]	74.00
HF [9]	73.00
Proposed method	**84.50**
Proposed method (+3° vein)	**84.75**

a bulls-eye test score of 84.50%, which is 3.75% higher than the second best IDSC + DP [5] method and 10.75% higher than the well-known SC [4] method.

V. CONCLUSION

Soybean cultivar classification is the first key step to facilitate soybean phenotype improvement needed for sustainable human and animal food production, energy production and environmental balance in agriculture worldwide. In this paper, we proposed a novel multiscale contour steered region integral method, in which the flexible interior (vein) connection structure, shape of the exterior contour, and their inter-relationship are effectively characterized at multiple scales to provide a comprehensive coarse-to-fine description of the leaf structure. The encouraging experimental results on the soybean cultivar leaf vein (SoyCultivarVein) database demonstrate the availability of cultivar information in leaf images and effectiveness of the proposed method for cultivar identification, which may advance the research in leaf shape analysis from species to cultivar. Also, the creation and public availability of the cultivar leaf vein database for the first time in the research community will enable on-going leaf-based cultivar classification, as well as providing the ground truth for research on automatic vein extraction. Solving the problem of extracting discriminative feature representations to further improve the cultivar classification performance would be an interesting and important topic for future work.

REFERENCES

[1] J. Schmutz *et al.*, "Genome sequence of the palaeopolyploid soybean," *Nature*, vol. 463, no. 7278, pp. 178–183, 2010.
[2] J. Wäldchen and P. Mäder, "Plant species identification using computer vision techniques: A systematic literature review," *Arch. Comput. Methods Eng.*, vol. 25, no. 2, pp. 507–543, 2018.
[3] J. S. Cope *et al.*, "Plant species identification using digital morphometrics: A review," *Expert Syst. Appl.*, vol. 39, no. 8, pp. 7562–7573, 2012.
[4] S. Belongie, J. Malik, and J. Puzicha, "Shape matching and object recognition using shape contexts," *IEEE Trans. Pattern Anal. Mach. Intell.*, vol. 24, no. 4, pp. 509–522, Apr. 2002.
[5] H. Ling and D. W. Jacobs, "Shape classification using the inner-distance," *IEEE Trans. Pattern Anal. Mach. Intell.*, vol. 29, no. 2, pp. 286–299, Feb. 2007.

[6] A. Srivastava, E. Klassen, S. H. Joshi, and I. H. Jermyn, "Shape analysis of elastic curves in Euclidean spaces," *IEEE Trans. Pattern Anal. Mach. Intell.*, vol. 33, no. 7, pp. 1415–1428, Jul. 2011.

[7] B. Wang and Y. Gao, "Hierarchical string cuts: A translation, rotation, scale, and mirror invariant descriptor for fast shape retrieval," *IEEE Trans. Image Process.*, vol. 23, no. 9, pp. 4101–4111, Sep. 2014.

[8] R. Hu, W. Jia, H. Ling, and D. Huang, "Multiscale distance matrix for fast plant leaf recognition," *IEEE Trans. Image Process.*, vol. 21, no. 11, pp. 4667–4672, Nov. 2012.

[9] J. Wang, X. Bai, X. You, W. Liu, and L. J. Latecki, "Shape matching and classification using height functions," *Pattern Recognit. Lett.*, vol. 33, no. 2, pp. 134–143, 2012.

[10] J. Park, E. Hwang, and Y. Nam, "Utilizing venation features for efficient leaf image retrieval," *J. Syst. Softw.*, vol. 81, no. 1, pp. 71–82, 2008.

[11] Y. Nam, E. Hwang, and D. Kim, "A similarity-based leaf image retrieval scheme: Joining shape and venation features," *Comput. Vis. Image Understand.*, vol. 110, no. 2, pp. 245–259, May 2008.

[12] L. Sack, E. M. Dietrich, C. M. Streeter, D. Sánchez-Gómez, and N. M. Holbrook, "Leaf palmate venation and vascular redundancy confer tolerance of hydraulic disruption," *Proc. Nat. Acad. Sci. USA*, vol. 105, no. 5, pp. 1567–1572, 2008.

[13] L. J. Hickey, "Classification of the architecture of dicotyledonous leaves," *Amer. J. Botany*, vol. 60, pp. 17–33, Jan. 1973.

[14] L. Sack *et al.*, "Developmentally based scaling of leaf venation architecture explains global ecological patterns," *Nature Commun.*, vol. 3, May 2012, Art. no. 837.

[15] H. Cochard, A. Nardini, and L. Coll, "Hydraulic architecture of leaf blades: Where is the main resistance?" *Plant, Cell Environ.*, vol. 27, no. 10, pp. 1257–1267, 2004.

[16] L. Sack and K. Frole, "Leaf structural diversity is related to hydraulic capacity in tropical rain forest trees," *Ecology*, vol. 87, no. 2, pp. 483–491, 2006.

[17] C. Scoffoni, M. Rawls, A. McKown, H. Cochard, and L. Sack, "Decline of leaf hydraulic conductance with dehydration: Relationship to leaf size and venation architecture," *Plant Physiol.*, vol. 156, no. 2, pp. 832–843, 2011.

[18] M. G. Larese, R. Namías, R. M. Craviotto, M. R. Arango, C. Gallo, and P. M. Granitto, "Automatic classification of legumes using leaf vein image features," *Pattern Recognit.*, vol. 47, no. 1, pp. 158–168, Jan. 2014.

[19] M. G. Larese, A. E. Bayá, R. M. Craviotto, M. R. Arango, C. Gallo, and P. M. Granitto, "Multiscale recognition of legume varieties based on leaf venation images," *Expert Syst. Appl.*, vol. 41, no. 10, pp. 4638–4647, 2014.

[20] H. Laga, S. Kurtek, A. Srivastava, M. Golzarian, and S. J. Miklavcic, "A riemannian elastic metric for shape-based plant leaf classification," in *Proc. Digit. Image Comput. Techn. Appl. (DICTA)*, Dec. 2012, pp. 1–7.

[21] L. Quan, P. Tan, G. Zeng, L. Yuan, J. Wang, and S. B. Kang, "Image-based plant modeling," *ACM Trans. Graph.*, vol. 25, no. 3, pp. 599–604, 2006.

[22] S. Mouine, I. Yahiaoui, and A. Verroust-Blondet, "Advanced shape context for plant species identification using leaf image retrieval," in *Proc. ACM Int. Conf. Multimedia Retr.*, 2012, Art. no. 49.

[23] G. Cerutti, L. Tougne, J. Mille, A. Vacavant, and D. Coquin, "A model-based approach for compound leaves understanding and identification," in *Proc. IEEE Int. Conf. Image Process. (ICIP)*, Sep. 2013, pp. 1471–1475.

[24] D. Bradley, D. Nowrouzezahrai, and P. Beardsley, "Image-based reconstruction and synthesis of dense foliage," *ACM Trans. Graph.*, vol. 32, no. 4, 2013, Art. no. 74.

[25] B. Wang, Y. Gao, C. Sun, M. Blumenstein, and J. La Salle, "Can walking and measuring along chord bunches better describe leaf shapes?" in *Proc. IEEE Conf. Comput. Vis. Pattern Recognit. (CVPR)*, Jul. 2017, pp. 6119–6128.

[26] C. Zhao, S. S. F. Chan, W.-K. Cham, and L. M. Chu, "Plant identification using leaf shapes—A pattern counting approach," *Pattern Recognit.*, vol. 48, no. 10, pp. 3203–3215, 2015.

[27] X. Yin, X. Liu, J. Chen, and D. M. Kramer, "Joint multi-leaf segmentation, alignment, and tracking for fluorescence plant videos," *IEEE Trans. Pattern Anal. Mach. Intell.*, vol. 40, no. 6, pp. 1411–1423, Jun. 2018.

[28] S. Kaul *et al.*, "Analysis of the genome sequence of the flowering plant *Arabidopsis thaliana*," *Nature*, vol. 408, no. 6814, pp. 796–815, 2000.

[29] L. J. Latecki and R. Lakämper, "Shape similarity measure based on correspondence of visual parts," *IEEE Trans. Pattern Anal. Mach. Intell.*, vol. 22, no. 10, pp. 1185–1190, Oct. 2000.

[30] H. Laga, S. Kurtek, A. Srivastava, and S. J. Miklavcic, "Landmark-free statistical analysis of the shape of plant leaves," *J. Theor. Biol.*, vol. 363, pp. 41–52, Dec. 2014.

[31] S. G. Wu, F. S. Bao, E. Y. Xu, Y.-X. Wang, Y.-F. Chang, and Q.-L. Xiang, "A leaf recognition algorithm for plant classification using probabilistic neural network," in *Proc. IEEE Int. Symp. Signal Process. Inf. Technol.*, Dec. 2007, pp. 11–16.

[32] O. Söderkvist, "Computer vision classification of leaves from Swedish trees," Ph.D. dissertation, Dept. Elect. Eng., Comput. Vis., Inst. Technol., Linköping Univ., Linköping, Sweden, 2001.

[33] H. Goëau *et al.*, "The ImageCLEF 2011 plant images classi cation task," in *Proc. ImageCLEF*, 2011, pp. 1–20.

[34] C. A. Price, O. Symonova, Y. Mileyko, T. Hilley, and J. S. Weitz, "Leaf extraction and analysis framework graphical user interface: Segmenting and analyzing the structure of leaf veins and areoles," *Plant Physiol.*, vol. 155, no. 1, pp. 236–245, 2011.

[35] A. Rosenfeld and J. L. Pfaltz, "Sequential operations in digital picture processing," *J. ACM*, vol. 13, no. 4, pp. 471–494, 1966.

[36] X. Bai, L. J. Latecki, and W.-Y. Liu, "Skeleton pruning by contour partitioning with discrete curve evolution," *IEEE Trans. Pattern Anal. Mach. Intell.*, vol. 29, no. 3, pp. 449–462, Mar. 2007.

[37] G. Borgefors, "Distance transformations in arbitrary dimensions," *Comput. Vis., Graph., Image Process.*, vol. 27, no. 3, pp. 321–345, 1984.

[38] D. Coeurjolly and A. Montanvert, "Optimal separable algorithms to compute the reverse Euclidean distance transformation and discrete medial axis in arbitrary dimension," *IEEE Trans. Pattern Anal. Mach. Intell.*, vol. 29, no. 3, pp. 437–448, Mar. 2007.

[39] T. E. Schouten and E. L. van den Broek, "Fast exact euclidean distance (FEED): A new class of adaptable distance transforms," *IEEE Trans. Pattern Anal. Mach. Intell.*, vol. 36, no. 11, pp. 2159–2172, Nov. 2014.

[40] S. R. Deans, *The Radon Transform and Some of Its Applications*. New York, NY, USA: Courier Corporation, 2007.

[41] K. Jafari-Khouzani and H. Soltanian-Zadeh, "Radon transform orientation estimation for rotation invariant texture analysis," *IEEE Trans. Pattern Anal. Mach. Intell.*, vol. 27, no. 6, pp. 1004–1008, Jun. 2005.

[42] Y. W. Chen and Y. Q. Chen, "Invariant description and retrieval of planar shapes using radon composite features," *IEEE Trans. Signal Process.*, vol. 56, no. 10, pp. 4762–4771, Oct. 2008.

[43] B. Wang and Y. Gao, "Structure integral transform versus radon transform: A 2D mathematical tool for invariant shape recognition," *IEEE Trans. Image Process.*, vol. 25, no. 12, pp. 5635–5648, Dec. 2016.

[44] X. Wang, G. Doretto, T. Sebastian, J. Rittscher, and P. Tu, "Shape and appearance context modeling," in *Proc. IEEE Int. Conf. Comput. Vis. (ICCV)*, Oct. 2007, pp. 1–8.

[45] R. Zhao, W. Ouyang, and X. Wang, "Unsupervised salience learning for person re-identification," in *Proc. IEEE Comput. Vis. Pattern Recognit. (CVPR)*, Jun. 2013, pp. 3586–3593.

[46] M. Köstinger, M. Hirzer, P. Wohlhart, P. M. Roth, and H. Bischof, "Large scale metric learning from equivalence constraints," in *Proc. IEEE Comput. Vis. Pattern Recognit. (CVPR)*, Jun. 2012, pp. 2288–2295.

[47] U. Park, Y. Tong, and A. K. Jain, "Age-invariant face recognition," *IEEE Trans. Pattern Anal. Mach. Intell.*, vol. 32, no. 5, pp. 947–954, May 2010.

[48] K. Chang, K. W. Bowyer, S. Sarkar, and B. Victor, "Comparison and combination of ear and face images in appearance-based biometrics," *IEEE Trans. Pattern Anal. Mach. Intell.*, vol. 25, no. 8, pp. 1160–1165, Sep. 2003.

[49] R. X. Hu, W. Jia, H. Ling, Y. Zhao, and J. Gui, "Angular pattern and binary angular pattern for shape retrieval," *IEEE Trans. Image Process.*, vol. 23, no. 3, pp. 1118–1127, Mar. 2014.

[50] N. Alajlan, M. S. Kamel, and G. H. Freeman, "Geometry-based image retrieval in binary image databases," *IEEE Trans. Pattern Anal. Mach. Intell.*, vol. 30, no. 6, pp. 1003–1013, Jun. 2008.

[51] H. V. Nguyen and F. Porikli, "Support vector shape: A classifier-based shape representation," *IEEE Trans. Pattern Anal. Mach. Intell.*, vol. 35, no. 4, pp. 970–982, Apr. 2013.

[52] X. Bai, C. Rao, and X. Wang, "Shape vocabulary: A robust and efficient shape representation for shape matching," *IEEE Trans. Image Process.*, vol. 23, no. 9, pp. 3935–3949, Sep. 2014.

XIAOHAN YU received the B.Sc. degree in computer science and technology from the Wuhan University of Technology, Wuhan, China, in 2013. He is currently pursuing the Ph.D. degree with the School of Engineering, Griffith University, Brisbane, QLD, Australia. His main research interests include plant image processing, computer vision, and pattern recognition.

YONGSHENG GAO received the B.Sc. and M.Sc. degrees in electronic engineering from Zhejiang University, Hangzhou, China, in 1985 and 1988, respectively, and the Ph.D. degree in computer engineering from Nanyang Technological University, Singapore. He is currently a Professor with the School of Engineering, Griffith University, and the Director of ARC Research Hub for driving farming productivity and disease prevention, Australia. He had been the Leader of the Biosecurity Group, Queensland Research Laboratory, National ICT Australia (ARC Centre of Excellence), a Consultant of Panasonic Singapore Laboratories, and an Assistant Professor with the School of Computer Engineering, Nanyang Technological University, Singapore. His research interests include smart farming, machine vision for agriculture, biosecurity, face recognition, image retrieval, computer vision, pattern recognition, environmental informatics, and medical imaging.

SHENGWU XIONG received the B.Sc. degree in computational mathematics and the M.Sc. and Ph.D. degree in computer software and theory from Wuhan University, Wuhan, China, in 1987, 1997, and 2003, respectively. He is currently a Professor with the School of Computer Science and Technology, Wuhan University of Technology, China. His research interests include intelligent computing, machine learning, and pattern recognition.

XIAOHUI YUAN received the B.Sc. and M.Sc. degrees in computer science from the Wuhan University of Technology, Wuhan, China, in 1999 and 2002, respectively, and the Ph.D. degree in applied mathematics from Hokkaido University, Japan, in 2007. He is currently a Professor with the School of Computer Science and Technology, Wuhan University of Technology. He had been the Leader and Principal Investigator of the Bioinformatics Group, Key Lab of Soybean Molecular Breeding, Northeast Institute of Geography and Agroecology, Chinese Academy of Sciences. His research interests include artificial intelligence and bioinformatics.